A general model for crack growth from initial defect in Very-High-Cycle Fatigue

Available online at www.sciencedirect.com

ScienceDirect

Procedia Structural Integrity 3 (2017) 411–423

Structural Integrity Procedia

www.elsevier.com/locate/procedia

XXIV Italian Group of Fracture Conference, 1-3 March 2017, Urbino, Italy

A general model for crack growth from initial defect in Very-High-Cycle Fatigue

Davide S. Paolino[a]*, Andrea Tridello[a], Giorgio Chiandussi[a], Massimo Rossetto[a]

[a]*Politecnico di Torino, Department of Mechanical and Aerospace Engineering, Corso Duca degli Abruzzi 24, Turin 10129, Italy*

Abstract

It is well-known in the literature that internal defects play a major role in the Very-High-Cycle Fatigue (VHCF) response of metallic materials. Generally, VHCF failures nucleate from internal defects characterized by a limited size. Unexpectedly, it has been found that cracks can grow from the initial defect even if the Stress Intensity Factor (SIF) is quite below the characteristic threshold for crack growth. Even though researchers unanimously accept this singular experimental evidence, they still dispute about its physical justification. Different micromechanical explanations have been proposed in the literature: local grain refinement, carbide decohesion, matrix fragmentation, hydrogen embrittlement, numerous cyclic pressure and formation of persistent slip bands are the most famous proposals. Regardless of the specific micromechanical explanation, it is generally acknowledged that a weakening mechanism occurs around the initial defect, thus permitting crack growth below the SIF threshold.

The present paper proposes an innovative approach for the quantitative modeling of the weakening process around the initial defect. The proposed model considers an additional SIF that reduces the SIF threshold of the material. Starting from a very general formulation for the additional SIF, possible scenarios for crack growth from the initial defect are also identified and described. It is theoretically demonstrated that, depending on the scenario, a VHCF limit may also be present and its final formulation recalls the well-known expression previously proposed by Murakami.

Peer-review under responsibility of the Scientific Committee of IGF Ex-Co.

Keywords: VHCF limit; SIF threshold; Crack growth

* Corresponding author. Tel.: +39-011-090-5746; fax: +39-011-090-6999.
E-mail address: davide.paolino@polito.it

Copyright © 2017 The Authors. Published by Elsevier B.V. This is an open access article under the CC BY-NC-ND license (http://creativecommons.org/licenses/by-nc-nd/4.0/).
Peer-review under responsibility of the Scientific Committee of IGF Ex-Co.
10.1016/j.prostr.2017.04.069

1. Introduction

The increasing demand for high performance machinery able to sustain significant loads for a very large number of cycles (larger than 10^8 cycles) is presently driving the research on the Very-High-Cycle Fatigue (VHCF) response of many metallic materials.

In the last decades, the extensive experimental investigation on VHCF has shown that failures mainly originate from internal defects (inclusions, pores and inhomogeneities) with a typical fish-eye morphology. Within the fish-eye, depending on the defect size and on the applied stress, fracture surfaces may show the so-called Fine Granular Area (FGA) in the vicinity of the internal defect. The FGA (also called Optically Dark Area or ODA by Murakami, Granular Bright Facet or GBF by Shiozawa and Rough Surface Area or RSA by Ochi) is a restricted region, dark at the optical microscope, that plays a key role in the initiation of the VHCF failure, since its formation consumes more than the 98% of the VHCF life. Researchers still dispute about the actual mechanism behind the FGA formation (Li et al., 2016), but they unanimously accept that, within the FGA, crack can grow even if the Stress Intensity Factor (SIF) is below the SIF threshold for crack growth.

In the present paper, the reduction of the SIF threshold within the FGA is originally modeled in agreement with the different weakening mechanisms proposed in the literature. Starting from a very general formulation for the SIF reduction, possible scenarios for crack growth from the initial defect are also identified and described. It is theoretically demonstrated that, depending on the scenario, a VHCF limit may also be present and its final formulation recalls the well-known expression previously proposed by Murakami (Murakami, 2002). An illustrative numerical example, based on experimental data, is finally reported in the paper in order to show the applicability of the proposed model and its potentialities.

Nomenclature

FGA	Fine Granular Area
HV	Vickers Hardness
SIF	Stress Intensity Factor
VHCF	Very-High-Cycle Fatigue
a_c , a_d , $a_{d,0}$, $a_{FGA,max}$, a_{FiE}	projected area of defects
$c_{th,g}$, $\alpha_{th,g}$, $c_{th,r}$, $\alpha_{th,r}$	parameters involved in SIF thresholds
c_I , m_I , c_{II} , m_{II} , c_{III} , m_{III} , c_s , m_s ,	Paris' constants in the three stages of crack growth
k_d	SIF of defect
$k_{th,g}$, $k_{th,l}$, $k_{th,r}$	SIF thresholds
s	stress amplitude
s_l	fatigue limit
N_f	number of cycles to failure
N_I , $N_{I,min}$, $N_{I,max}$, N_{II} , N_{III}	number of cycles in the three stages of crack growth

2. Methods

A general expression for modeling the SIF threshold within the FGA is presented in Section 2.1. Starting from the proposed model, an expression for the fatigue limit is defined in Section 2.2 and a model for the crack growth rate is introduced in Section 2.3.

2.1. SIF threshold within the FGA

It is generally acknowledged that crack can grow within the FGA even if the SIF is below the SIF threshold of the material. Regardless of the physical justification for this unexpected experimental evidence, crack growth can occur in the FGA only if a local reduction of the global SIF threshold of the material is accepted.

The following assumptions permit to define a general model for the local reduction of the SIF threshold within the FGA:

1. the global SIF threshold, referred to as $k_{th,g}$, can be expressed as (Shiozawa et al. 2001; Murakami, 2002; Tanaka and Akiniwa, 2002; Chapetti et al., 2003; Liu et al., 2006; Li et al., 2010; Hong et al., 2014; Matsunaga et al., 2015):

$$k_{th,g} = c_{th,g}\left(HV + 120\right)\sqrt{a_d}^{\alpha_{th,g}}, \tag{1}$$

where a_d is the projected area of the defect, HV is the Vickers hardness of the material in the vicinity of the defect and $c_{th,g} > 0$ and $0 \le \alpha_{th,g} < 1/2$ (being $\alpha_{th,g} = 0$ in case of global SIF threshold for long cracks) are two material coefficients.

2. the SIF for an internal defect, referred to as k_d, is given by (Murakami, 2002):

$$k_d = 0.5s\sqrt{\pi}\sqrt{a_d}^{1/2}, \tag{2}$$

where s is the local stress amplitude at the defect location.

3. within the FGA, the local SIF threshold, referred to as $k_{th,l}$, is defined as:

$$k_{th,l} = k_{th,g} - k_{th,r}, \tag{3}$$

where $k_{th,r}$ accounts for the reduction of the SIF threshold induced by the different weakening mechanisms proposed in the literature: local grain refinement (Sakai, 2009; Nakamura et al., 2010; Grad et al., 2012; Sakai et al, 2015; Hong et al., 2016), hydrogen embrittlement (Murakami, 2002; Liu et al., 2010), carbide decohesion (Shiozawa et al., 2001), matrix fragmentation (Shanyavskiy, 2013) or formation of persistent slip bands (Huang et al., 2010).

4. the SIF threshold reduction has the most general formulation fulfilling the following three basic conditions:
    a. the principle of dimensional homogeneity, for which $k_{th,r}$ must be proportional to the stress amplitude and to the square-root of the defect size.
    b. the initial condition, for which $k_{th,r}$ must be proportional to the square-root of the initial defect size when crack starts growing.
    c. the defect size dependency, for which $k_{th,r}$ may depend on the defect size.

According to the conditions a)-c), the easiest and most general formulation for $k_{th,r}$ is:

$$k_{th,r} = c_{th,r} s \sqrt{a_{d,0}}^{1/2} \left(\sqrt{a_d} / \sqrt{a_{d,0}} \right)^{\alpha_{th,r}}, \tag{4}$$

where $a_{d,0}$ is the projected area of the initial defect and $c_{th,r} \geq 0$ and $\alpha_{th,r} \leq 0$ (being $\alpha_{th,r} = 0$ if $k_{th,r}$ is a constant value) are two material coefficients that ensure $0 \leq k_{th,l} \leq k_{th,g}$ for any $\sqrt{a_d}$ value.

5. FGA forms until $k_{th,l} < k_d \leq k_{th,g}$.

From Eqs. (1), (3) and (4), the general expression for the local SIF threshold is finally given by:

$$k_{th,l} = c_{th,g} \left(HV + 120 \right) \sqrt{a_d}^{\alpha_{th,g}} - c_{th,r} s \sqrt{a_{d,0}}^{1/2} \left(\sqrt{a_d} / \sqrt{a_{d,0}} \right)^{\alpha_{th,r}}. \tag{5}$$

2.2. Fatigue limit expression

According to assumption 5) in Section 2.1, the following four distinct cases may occur:

1. $k_d \left(\sqrt{a_{d,0}} \right) > k_{th,g} \left(\sqrt{a_{d,0}} \right)$: fatigue life is finite and the FGA does not form. Crack grows until failure without the assistance of any weakening mechanism.
2. $k_{th,l} \left(\sqrt{a_{d,0}} \right) < k_d \left(\sqrt{a_{d,0}} \right) \leq k_{th,g} \left(\sqrt{a_{d,0}} \right)$: fatigue life is finite, the FGA forms and it reaches its maximum extension, $\sqrt{a_{FGA,max}}$. Within the FGA, crack can grow thanks to the weakening mechanisms proposed in the literature (Shiozawa et al., 2001; Murakami, 2002; Sakai, 2009; Huang et al., 2010; Liu et al., 2010; Nakamura et al., 2010; Grad et al., 2012; Shanyavskiy, 2013; Sakai et al, 2015; Hong et al., 2016). When k_d reaches $k_{th,g}$, the FGA attains its maximum extension. Then crack grows until failure without the assistance of any weakening mechanism.
3. $k_{th,l} \left(\sqrt{a_{d,0}} \right) < k_d \left(\sqrt{a_{d,0}} \right) \leq k_{th,g} \left(\sqrt{a_{d,0}} \right)$: fatigue life is infinite, the FGA forms but it does not reach the maximum extension. Within the FGA, crack can grow thanks to any of the weakening mechanisms proposed in the literature (Shiozawa et al., 2001; Murakami, 2002; Sakai, 2009; Huang et al., 2010; Liu et al., 2010; Nakamura et al., 2010; Grad et al., 2012; Shanyavskiy, 2013; Sakai et al, 2015; Hong et al., 2016). When $k_{th,l}$ reaches k_d, the FGA stops forming at $\sqrt{a_{FGA}} < \sqrt{a_{FGA,max}}$ and crack arrests.
4. $k_d \left(\sqrt{a_{d,0}} \right) \leq k_{th,l} \left(\sqrt{a_{d,0}} \right)$: fatigue life is infinite and the FGA does not form. Crack cannot grow from the initial defect.

Fig. 1 qualitatively depicts the four cases in a double logarithmic plot of the SIF with respect to the defect size.

The transition between case 2) and case 3) discriminates between finite and infinite fatigue life and it occurs when, for a given initial defect size, the stress amplitude equals the material fatigue limit. It can be demonstrated (Paolino et al., 2016) that the material fatigue limit, referred to as s_l, can be expressed as:

$$s_l = c_{s_l} \frac{c_{th,g} \left(HV + 120 \right)}{\sqrt{a_{d,0}}^{1/2 - \alpha_{th,g}}}, \tag{6}$$

where $c_{s_l} = \left(\frac{\left(1/2-\alpha_{th,g}\right)0.5\sqrt{\pi}}{\left(\alpha_{th,g}-\alpha_{th,r}\right)c_{th,r}} \right)^{\frac{1/2-\alpha_{th,g}}{1/2-\alpha_{th,r}}} \frac{\alpha_{th,g}-\alpha_{th,r}}{0.5\sqrt{\pi}\left(1/2-\alpha_{th,r}\right)}$. Eq. (6) recalls the well-known expression proposed by Murakami (Murakami, 2002) and it can be obtained by imposing the condition of tangency (Fig. 2) between the $k_d\left(\sqrt{a_d}\right)$ curve (Eq. (1)) and the $k_{th,l}\left(\sqrt{a_d}\right)$ curve (Eq. (5)).

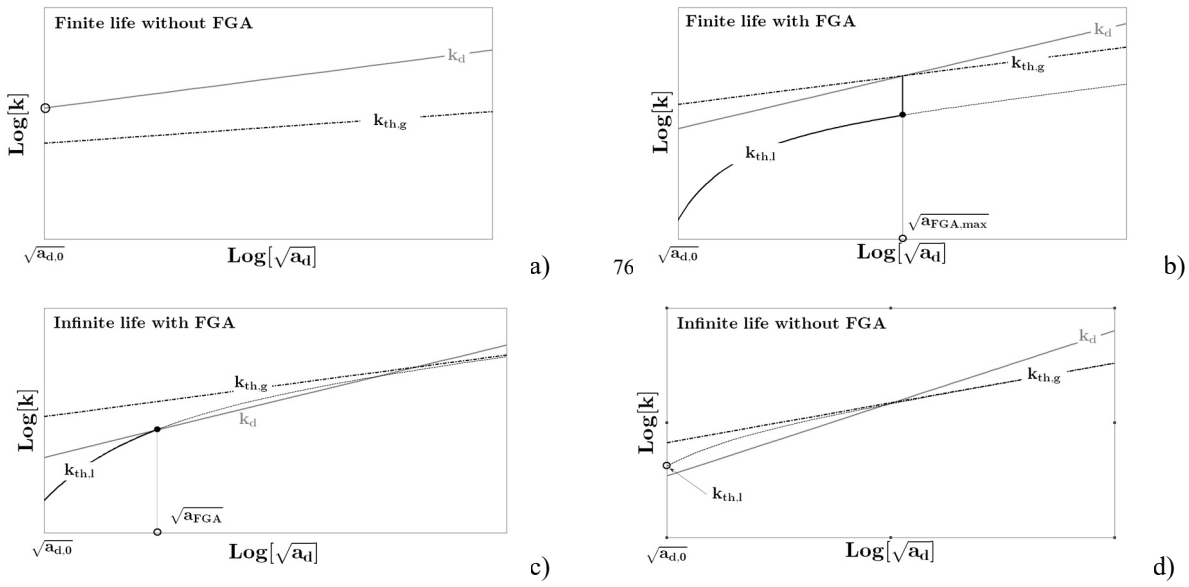

Fig. 1. Variation of relevant SIFs with defect size in VHCF: a) Finite life without FGA formation; b) Finite life with FGA formation; c) Infinite life with FGA formation; d) Infinite life without FGA formation.

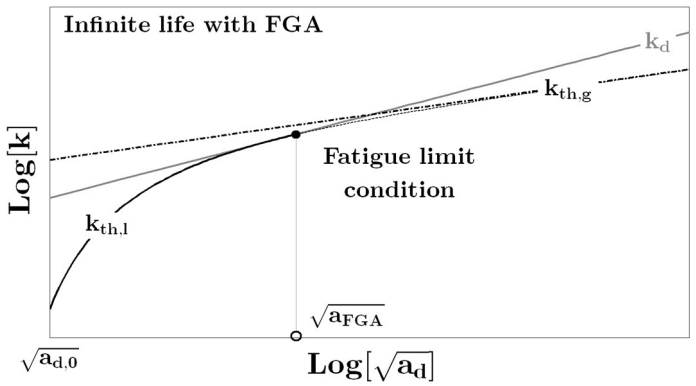

Fig. 2. Variation of relevant SIFs with defect size in fatigue limit condition.

2.3. Crack growth rate within the FGA

In the VHCF literature (Tanaka and Akiniwa, 2002; Marines-Garcia et al., 2008; Su et al., in press), the crack growth rate within the FGA is usually modeled with the Paris' law. Three stages can be present in sigmoidal crack growth rate diagrams related to VHCF failures from internal defects (see Fig. 3): the below-threshold region within

the FGA (up to $k_{th,g}$), the steady crack propagation region from the border of the FGA (with SIF equal to $k_{th,g}$) to the border of the fish-eye (with SIF equal to k_{FiE}), the unsteady crack propagation region beyond the fish-eye border (with SIF larger than k_{FiE}).

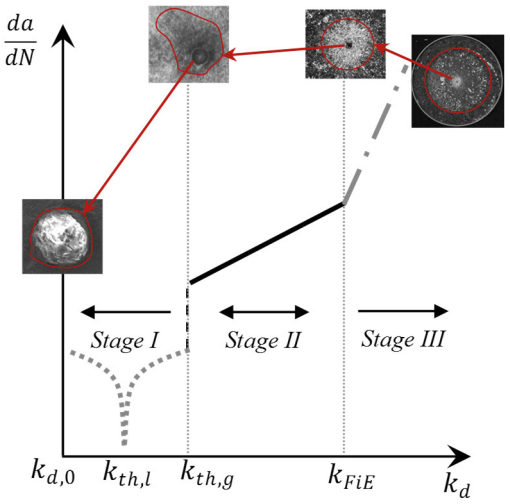

Fig. 3. The three stages of crack propagation in a crack growth rate diagram for VHCF failures from internal defects.

In order to model the below-threshold region, the modified Paris' law proposed by Donahue et al. (1972) (see also Sun et al., 2014) is here adopted (a stress ratio equal to -1 is assumed in the following, yielding the effective stress equal to the stress amplitude):

$$\frac{da}{dN} = c_I \left(k_d - k_{th,l}\right)^{m_I}, \tag{7}$$

where c_I and m_I are the two Paris' constants related to the first propagation stage, from $\sqrt{a_{d,0}}$ to $\sqrt{a_{FGA,max}}$.

From the border of the FGA to the border of the fish-eye (with size $\sqrt{a_{FiE}}$), the crack growth rate is modeled with the conventional Paris' law, in agreement with the literature (Tanaka and Akiniwa, 2002; Marines-Garcia et al., 2008; Su et al., in press):

$$\frac{da}{dN} = c_{II} k_d^{m_{II}}, \tag{8}$$

where c_{II} and m_{II} are the two Paris' constants related to the second propagation stage, from $\sqrt{a_{FGA,max}}$ to $\sqrt{a_{FiE}}$.

Final fracture may occur when the crack size reaches the border of the fish-eye. In these cases, the third stage of crack propagation is not visible on fracture surfaces and it can be neglected. In some other cases, crack can propagate beyond the fish-eye border until it reaches the border of the final fracture, with size $\sqrt{a_c}$. . In these cases, a third stage of crack propagation is visible on fracture surfaces and it can be modeled again with the conventional Paris' law (Su et al., in press):

$$\frac{da}{dN} = c_{III} k_d^{m_{III}} , \tag{9}$$

where c_{III} and m_{III} are the two Paris' constants related to the third propagation stage, from $\sqrt{a_{FiE}}$ to $\sqrt{a_c}$.

By taking into account the three stages of propagation, the number of cycles to failure, N_f , can be expressed as:

$$N_f = N_I + N_{II} + N_{III} , \tag{10}$$

where N_I , N_{II} . and N_{III} are the number of cycles consumed within stages I, II and III, respectively.

Following the procedure usually adopted in the VHCF literature (e.g., Su et al., in press), N_I can be estimated by subtracting, from the experimental N_f , the number of cycles N_{II} and N_{III} obtained through integration of Eqs. (8) and (9). The Paris' constants in Eq. (8) are those typical for surface cracks in the steady phase of crack growth; whereas, the Paris' constants in Eq. (9) are for surface cracks in the unsteady phase of crack growth, near the final fracture. If the Paris' constants in Eq. (9) are assumed equal to those of Eq. (8), the crack growth rate is underestimated and, consequently, N_{III} is overestimated. Therefore, it can be concluded that:

$$N_{I,min} = N_f - N_{II-III} < N_I < N_f - N_{II} = N_{I,max} , \tag{11}$$

where

$$\begin{cases} N_{II-III} = \dfrac{\sqrt{a_c}^{1-m_s/2} - \sqrt{a_{FGA,max}}^{1-m_s/2}}{\left(1-m_s/2\right) c_s \left(0.5 s \sqrt{\pi}\right)^{m_s}} \\ N_{II} = \dfrac{\sqrt{a_{FiE}}^{1-m_s/2} - \sqrt{a_{FGA,max}}^{1-m_s/2}}{\left(1-m_s/2\right) c_s \left(0.5 s \sqrt{\pi}\right)^{m_s}} \end{cases} , \tag{12}$$

being c_s and m_s the two Paris' constants for surface cracks in the steady phase of crack growth.

The difference between $N_{I,min}$ and $N_{I,max}$ is generally negligible if N_f is larger than 10^8 cycles. Thus, the average value between $N_{I,min}$ and $N_{I,max}$ is a good approximation for . N_I ..

The approximated experimental N_I values can be used for the estimation of the four parameters c_I , m_I , $c_{th,r}$ and $\alpha_{th,r}$: according to nonlinear least squares method, the parameter estimates are obtained by minimizing the sum of squared percent errors between the experimental $\log_{10}\left(N_I\right)$ values and the $\log_{10}\left(N_I\right)$ values computed through integration of Eq. (7). The other two parameters involved in Eq. (7) (i.e., $c_{th,g}$ and $\alpha_{th,g}$) are estimated through application of the ordinary least squares method to the experimental data related to the $\sqrt{a_{FGA,max}}$ values measured on the fracture surfaces. In particular, $c_{th,g}$ and $\alpha_{th,g}$ are obtained with a linear fit of the $k_d\left(\sqrt{a_{FGA,max}}\right)$ values vs. the $\sqrt{a_{FGA,max}}$ values, in a log-log plot (Paolino et al., 2016).

3. Application to an experimental dataset

In order to show the applicability of the proposed approach, model parameters are fitted to an experimental dataset.

VHCF tests are carried out on Gaussian specimens (Paolino et al., 2014) made of an AISI H13 steel with Vickers hardness 560 kg_f/mm^2. Details on the testing setup and on the tested material are reported in Tridello et al. (2015) and Tridello et al. (2016) and will not be recalled here for the sake of brevity. Twelve specimens are loaded at a constant stress amplitude up to failure. The number of cycles to failure ranges from $4.2 \cdot 10^7$ to $3.85 \cdot 10^9$ cycles. Fracture surfaces are seen through a Scanning-Electron-Microscope (SEM) in order to measure the initial defect size (i.e., $\sqrt{a_{d0}}$) in each specimen; whereas, the FGA sizes (i.e., $\sqrt{a_{FGA,max}}$) are measured from pictures taken at the optical microscope. From the SEM analysis, all the fatigue fractures nucleated from non-metallic inclusions (oxide-type inclusions).

The local stress amplitude in the vicinity of the initial defect is considered as the stress amplitude applied during the test. As shown in the S-N plot of the experimental dataset (Fig. 4), the local stress amplitudes are in the range 500 – 635 MPa.

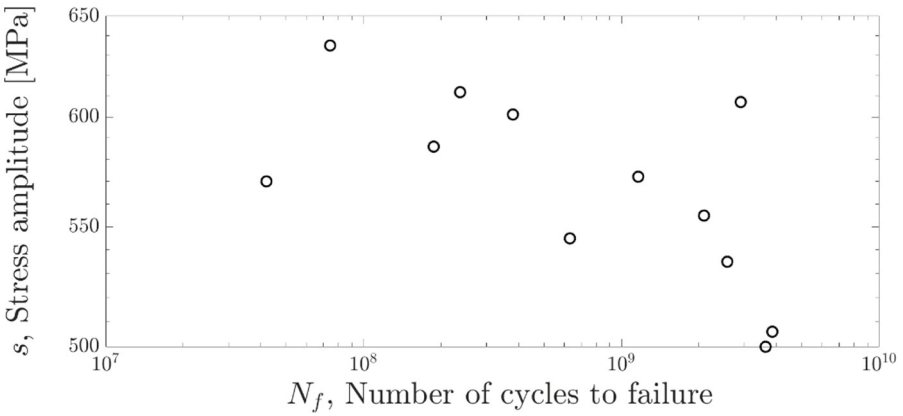

Fig. 4. S-N plot of the experimental dataset.

As a first step, the parameters and are estimated from the FGA sizes. As shown in Fig. 5, the linear model of Eq. (1) is in good agreement with the experimental data.

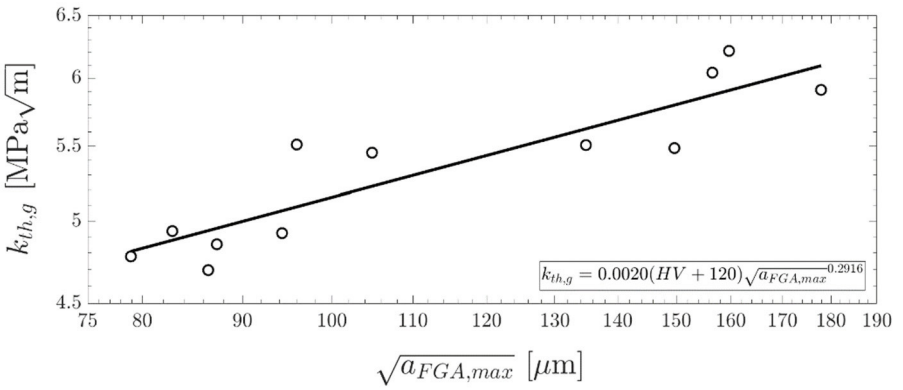

Fig. 5. Global SIF threshold variation as a function of the FGA size.

In particular, according to Eq. (1), the least squares estimates of $c_{th,g}$ and $\alpha_{th,g}$ are given by:

$$\begin{cases} \widetilde{c_{th,g}} = 1.979 \cdot 10^{-3} \\ \widetilde{\alpha_{th,g}} = 0.2916 \end{cases}, \tag{13}$$

where $\tilde{\cdot}$ denotes the parameter estimate. It is worth noting that the estimates $\widetilde{c_{th,g}}$ and $\widetilde{\alpha_{th,g}}$ are in agreement with the values proposed in the literature for $c_{th,g}$ (Li et al., 2010; Liu et al., 2008) and for $\alpha_{th,g}$ (Murakami, 2002; Liu et al., 2008; Li et al., 2010; Matsunaga et al., 2015).

In order to estimate c_I, m_I, $c_{th,r}$ and $\alpha_{th,r}$, the experimental number of cycles consumed in stage I must be computed from Eqs. (11) and (12). The two Paris' constants in Eq. (12) (i.e., c_s =4.6·10^{-12} and $m_s = 3.21$) are taken from the available literature (Schuchtar and Plumtree, 1988) for a very similar steel type. Fig. 6 shows the variation of the ratios of $N_{I,min} / N_f$ and $N_{I,max} / N_f$ with N_f.

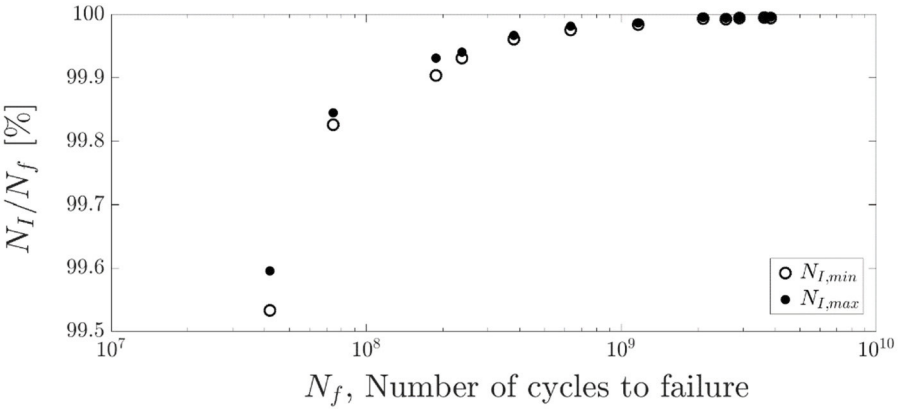

Fig. 6. Variation of the ratios and with the number of cycles to failure.

As shown in Fig. 6, the difference between $N_{I,min}$ and $N_{I,max}$ is negligible. Therefore, the average value between $N_{I,min}$ and $N_{I,max}$ can be considered as a good approximation of the actual N_I. In agreement with the literature (Tanaka and Akiniwa, 2002; Hong et al., 2014; Su et al., in press), the ratio N_I / N_f increases rapidly with N_f and, for the experimental dataset, is larger than 99.5%. From the experimental N_I values and from the measured $\sqrt{a_{d,0}}$ and $\sqrt{a_{FGA,max}}$ values, it is also possible to compute the average crack growth rate within stage I:

$$\overline{v_{a,I}} = \frac{\sqrt{a_{FGA,max}} - \sqrt{a_{d,0}}}{N_I}, \tag{14}$$

where $\overline{v_{a,I}}$ denotes the average da/dN in stage I. Fig. 7 shows the variation of $\overline{v_{a,I}}$ with N_f.

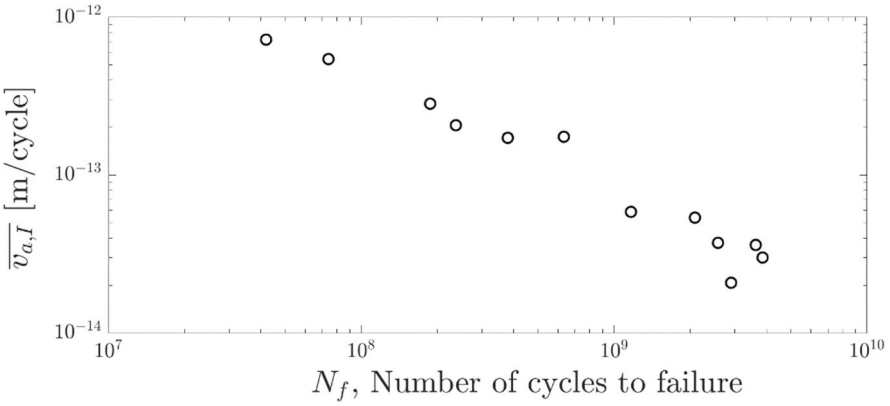

Fig. 7. Variation of the average crack growth rate within stage I with the number of cycles to failure.

As shown in Fig. 7, the crack growth rate decreases with the number of cycles to failure. It is worth noting that, for N_f larger than 10^9, the crack growth rate is smaller than the physical threshold of 10^{-13} m/cycle suggested by Pippan et al. (2002) and is far below one Burgers' vector (Tanaka and Akiniwa, 2002; Zhao et al., 2011; Sun et al., 2014). Therefore, it can be argued that crack growth within the FGA is not uniform: crack alternatively arrests and grows with an average rate that can be smaller than 10^{-13} m/cycle.

Application of the nonlinear least squares method yields the following estimates for parameters c_I, m_I, $c_{th,r}$ and $\alpha_{th,r}$:

$$\begin{cases} \widetilde{c_I} = 2.908 \cdot 10^{-15} \\ \widetilde{m_I} = 4.249 \\ \widetilde{c_{th,r}} = 0.8966 \\ \widetilde{\alpha_{th,r}} = -0.2175 \end{cases}, \tag{15}$$

Fig. 8 shows the good agreement obtained between the experimental and the estimated values of N_I and $\overline{v_{a,I}}$, after the fitting procedure.

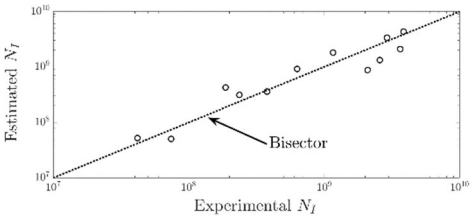

a)

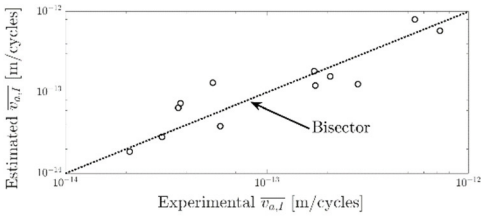

b)

Fig. 8. Comparison between estimated and experimental data: a) Number of cycles consumed in stage I; b) Average crack growth rate in stage I.

From the estimates in Eqs. (13) and (15), it is also possible to estimate an average fatigue limit, according to the expression in Eq. (6). The fatigue limit depends on the initial defect size. Fig. 9 shows the variation of the fatigue limit with the initial defect size, for the experimental dataset.

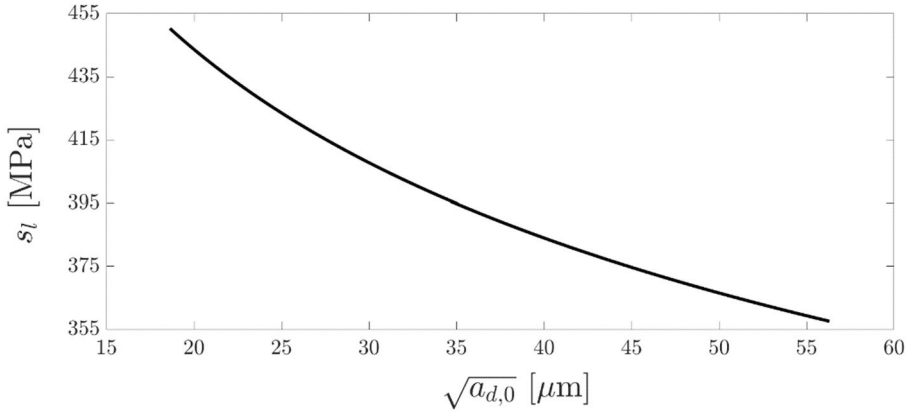

Fig. 9. Variation of the fatigue limit with the initial defect size.

As shown in Fig. 9 and reported in the literature (Murakami, 2002; Furuya, 2011), the fatigue limit decreases with the initial defect size. As expected from the definition of fatigue limit, the values in Fig. 9 are far below the stress amplitudes that induce failure for the investigated material.

Depending on the stress amplitude and on the initial defect size, the different scenarios in Figs. (1) and (2) may occur. Fig. (10) shows the Paris' diagram for an initial defect size equal to 40 μm and for different relevant values of the stress amplitude.

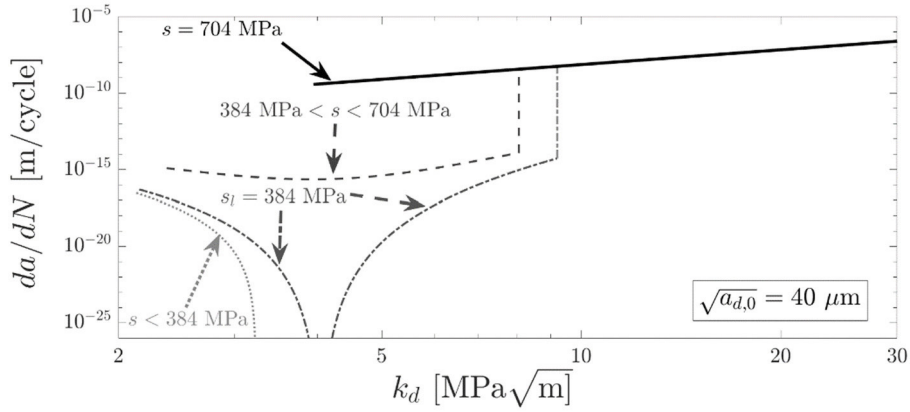

Fig. 10. Variation of the fatigue limit with the initial defect size.

As shown in Fig. (10), for stress amplitudes below the fatigue limit of 384 MPa the crack arrests and the fatigue life is infinite. In particular, for stress amplitudes below 350 MPa, the FGA does not form; whereas, in the range 350 – 384 MPa, the FGA forms but it does not reach its maximum size. For stress amplitudes above the fatigue limit, the crack does not arrest and the fatigue life is finite. In particular, for stress amplitudes larger than 704 MPa, the FGA does not form; whereas, in the range 384 – 704 MPa the FGA forms and it reaches its maximum size.

4. Conclusions

A simple and general formulation for the reduction of the SIF threshold in the FGA was proposed in the paper. It was shown that, with the proposed formulation, the different weakening mechanisms involved in the FGA formation

can be quantitatively modeled. From the proposed formulation, a general expression for the fatigue limit and a crack growth rate model for crack propagation from internal defect up to failure were defined. The procedure for the estimation of the six parameters in the crack growth rate model was also shown.

The model was successfully applied to an experimental dataset. The estimated and the experimental average crack growth rates within the FGA were found to be far below the physical threshold for crack growth. This experimental evidence suggested that crack does not grow uniformly within the FGA and that it rather alternates arrest and propagation phases.

References

Chapetti, M. D., Tagawa, T., Miyata, T., 2003. Ultra-long cycle fatigue of high-strength carbon steels part II: estimation of fatigue limit for failure from internal inclusions. Materials Science and Engineering: A 356, 236-244.

Donahue, R. J., Clark, H. M., Atanmo, P., Kumble, R., McEvily, A. J., 1972. Crack opening displacement and the rate of fatigue crack growth. International Journal of Fracture Mechanics 8, 209-219.

Furuya, Y., 2011. Notable size effects on very high cycle fatigue properties of high-strength steel. Materials Science and Engineering: A 528, 5234-5240.

Grad, P., Reuscher, B., Brodyanski, A., Kopnarski, M., Kerscher, E., 2012. Mechanism of fatigue crack initiation and propagation in the very high cycle fatigue regime of high-strength steels. Scripta Materialia 67, 838-841.

Hong, Y., Lei, Z., Sun, C., Zhao, A., 2014. Propensities of crack interior initiation and early growth for very-high-cycle fatigue of high strength steels. International Journal of Fatigue 58, 144-151.

Hong, Y., Liu, X., Lei, Z., Sun, C., 2016. The formation mechanism of characteristic region at crack initiation for very-high-cycle fatigue of high-strength steels. International Journal of Fatigue 89, 108-118.

Huang, Z., Wagner, D., Bathias, C., Paris, P. C., 2010. Subsurface crack initiation and propagation mechanisms in gigacycle fatigue. Acta Materialia 58, 6046-6054.

Li, Y. D., Zhang, L. L., Fei, Y. H., Liu, X. Y., Li, M. X., 2016. On the formation mechanisms of fine granular area (FGA) on the fracture surface for high strength steels in the VHCF regime. International Journal of Fatigue 82, 402-410.

Li, W., Sakai, T., Li, Q., Lu, L. T., Wang, P., 2010. Reliability evaluation on very high cycle fatigue property of GCr15 bearing steel. International Journal of Fatigue 32, 1096-1107.

Liu, Y. B., Yang, Z. G., Li, Y. D., Chen, S. M., Li, S. X., Hui, W. J., Weng, Y. Q., 2008. On the formation of GBF of high-strength steels in the very high cycle fatigue regime. Materials Science and Engineering: A 497, 408-415.

Liu, Y. B., Li, Y. D., Li, S. X., Yang, Z. G., Chen, S. M., Hui, W. J., Weng, Y. Q., 2010. Prediction of the S–N curves of high-strength steels in the very high cycle fatigue regime. International journal of fatigue 32, 1351-1357.

Marines-Garcia, I., Paris, P. C., Tada, H., Bathias, C., Lados, D., 2008. Fatigue crack growth from small to large cracks on very high cycle fatigue with fish-eye failures. Engineering Fracture Mechanics 75, 1657-1665.

Matsunaga, H., Sun, C., Hong, Y., Murakami, Y., 2015. Dominant factors for very-high-cycle fatigue of high-strength steels and a new design method for components. Fatigue & Fracture of Engineering Materials & Structures 38, 1274-1284.

Murakami, Y., 2002. *Metal fatigue: effects of small defects and nonmetallic inclusions*. Elsevier, Oxford, UK.

Nakamura, T., Oguma, H., Shinohara, Y., 2010. The effect of vacuum-like environment inside sub-surface fatigue crack on the formation of ODA fracture surface in high strength steel. Procedia Engineering 2, 2121-2129.

Paolino, D. S., Tridello, A., Chiandussi, G., Rossetto, M., 2014. On specimen design for size effect evaluation in ultrasonic gigacycle fatigue testing. Fatigue & Fracture of Engineering Materials & Structures 37, 570-579.

Paolino, D. S., Tridello, A., Chiandussi, G., Rossetto, M., 2016. S-N curves in the very-high-cycle fatigue regime: statistical modeling based on the hydrogen embrittlement consideration. Fatigue & Fracture of Engineering Materials & Structures 39, 1319-1336.

Pippan, R., Tabernig, B., Gach, E., Riemelmoser, F., 2002. Non-propagation conditions for fatigue cracks and fatigue in the very high-cycle regime. Fatigue & Fracture of Engineering Materials & Structures 25, 805-811.

Sakai, T., 2009. Review and prospects for current studies on very high cycle fatigue of metallic materials for machine structural use. Journal of solid mechanics and materials engineering 3, 425-439.

Sakai, T., Oguma, N., Morikawa, A., 2015. Microscopic and nanoscopic observations of metallurgical structures around inclusions at interior crack initiation site for a bearing steel in very high-cycle fatigue. Fatigue & Fracture of Engineering Materials & Structures 38, 1305-1314.

Schuchtar, E., Plumtree, A., 1988. Temperature and Frequency Effects on Fatigue Crack Propagation. ECF 7. Failure Analysis – Theory and Practice 2, 1081-1086.

Shanyavskiy, A. A., 2013. Mechanisms and modeling of subsurface fatigue cracking in metals. Engineering Fracture Mechanics 110, 350-363.

Shiozawa, K., Lu, L., Ishihara, S., 2001. S–N curve characteristics and subsurface crack initiation behaviour in ultra-long life fatigue of a high carbon-chromium bearing steel. Fatigue & Fracture of Engineering Materials & Structures 24, 781-790.

Su, H., Liu, X., Sun, C., Hong, Y., in press. Nanograin layer formation at crack initiation region for very-high-cycle fatigue of a Ti–6Al–4V alloy. Fatigue & Fracture of Engineering Materials & Structures.

Sun, C., Lei, Z., Hong, Y., 2014. Effects of stress ratio on crack growth rate and fatigue strength for high cycle and very-high-cycle fatigue of metallic materials. Mechanics of Materials 69, 227-236.

Tanaka, K., Akiniwa, Y., 2002. Fatigue crack propagation behaviour derived from S–N data in very high cycle regime. Fatigue & Fracture of Engineering Materials & Structures 25 775-784.

Tridello, A., Paolino, D. S., Chiandussi, G., Rossetto, M., 2015. VHCF response of AISI H13 steel: assessment of size effects through Gaussian specimens. Procedia Engineering 109, 121-127.

Tridello, A., Paolino, D. S., Chiandussi, G., Rossetto, M., 2016. Different inclusion contents in H13 steel: Effects on VHCF response of Gaussian specimens. Key Engineering Materials 665, 49-52.

Zhao, A., Xie, J., Sun, C., Lei, Z., Hong, Y., 2011. Prediction of threshold value for FGA formation. Materials Science and Engineering: A 528, 6872-6877.